STUDIA UBB CHEMIA, LXIX, 1, 2024 (p. 35-50)
(RECOMMENDED CITATION)
DOI:10.24193/subbchem.2024.1.03

TUNGSTATE-BORATE IONIC LIQUIDS: STRUCTURE, ELECTROCHEMICAL BEHAVIOR AND ELECTRODEPOSITION OF TUNGSTEN COATINGS

Angelina GAB[a], Victor MALYSHEV[a], Dmytro SHAKHNIN[a], Ana-Maria POPESCU[b*], Virgil CONSTANTIN[b*]

ABSTRACT. This work was undertaken to study the electrodeposition of tungsten from the Na_2WO_4-B_2O_3 system in the molten state. The measurement of the EMF being made with platinum-oxygen indicator and tungsten relative electrodes versus platinum-oxygen.

Experiment due to dependencies of the platinum-oxygen potential and tungsten electrodes on the B_2O_3 concentration, are validate by the forming of ditungstate ions $W_2O_7^{2-}$ in the high temperature ionic liquids (HTILs).The electroreduction process of the active species, is controlled by the diffusion; the rate of formation of the active species does not limit the electrode process; Polarization, in galvanostatic and potentiodynamic mode, have highlighted the fact that charge transfer is reversible.

In the Na_2WO_4-B_2O_3 melt (acid-basic character), in a narrow potential range and at a controlled process potential, the electroreduction of tungsten from its dimeric form is possible due to the multielectronic processes that take place at the electrode surface. This study played an important role in the evolution tungsten coatings; the corrosion potentials of electrodes (copper, nickel, steel) plated with tungsten, were also measured.

In this study, the influence of some parameters (temperature, electrolysis time, cathodic current density, B_2O_3 concentration) on the cathodic structure and composition was quantified, determining the optimal conditions of the reverse electrodeposition.

Keywords: *Tungstate, Borate, Ionic liquid, Electrodeposition, Voltammetry*

[a] *International European University, 42 V Academician Glushkov Avenue, 03187, Kyiv, Ukraine*
[b] *Romanian Academy, "Ilie Murgulescu" Institute of Physical Chemistry, Laboratory of Electrochemistry and Corrosion, 202 Splaiul Independentei, 060021, Bucharest, Romania*
* *Corresponding authors: virgilconstantin@yahoo.com, popescuamj@yahoo.com*

INTRODUCTION

Increased interest in the development of new effective methods for obtaining refractory compounds such as carbides, borides, silicides, alloys, and intermetallic compounds of Groups IV–VIB of the periodic table is dictated by their use in modern technique. A comparative analysis of the synthesis of metal-like refractory compounds showed that high-temperature electrochemical synthesis (HTES) is one of the most promising but still poorly known methods and it is based on processes of the electrical separation of metals and nonmetals from ion melts [1–3]. These coatings are characterized by yet another important feature, that is, they are economically profitable because in some cases their use allows simplifying the technology and replacing expensive and rare metals by more abundant metals without any sacrifice in the operation of parts, structures, and aggregates.

Vast family of highly prospective and widely used ionic liquids encompasses, among all, high-temperature ionic liquids (HTILs) inorganic salts systems, in particular tungstate-borate (Na2WO4-B2O3) melts Acid-base properties of tungstate HTILs have substantial effect both on electrode processes and composition of cathodic products. Various acceptors of oxygen ions, such as cations Li^+, Ca^{2+}, Mg^{2+}, Zn^{2+}, Al^{3+} anions PO^{3-}, and neutral molecules WO_3, MoO_3, CO_2, were used to modify acidity of the melts [4-7]. The cations of alkali and alkaline-earth metals form cationized electrochemically active species while PO^{3-}, WO_3, MoO_3, CO_2 produce dimeric complexes. Earlier we studied peculiarities of molybdenum and tungsten different ionic forms in tungstate melt in the presence of strong-polarizing cations: Li^+, Ca^{2+}, Mg^{2+}, Zn^{2+}, Al^{3+}, neutral molecules WO_3, MoO_3, and CO_2, anions PO^{3-} [6-8]. Investigations showed that it is possible to realize multielectron equilibria and processes with the use of acid-base interactions in sodium tungstate melt. Depending on the acid-base properties of the melt, cathode products can be tungsten, its oxides, and/or tungsten bronzes. The possibility of electrodeposition of tungsten in the form of dispersed powders or coatings in the presence of a parallel process of electroreduction of a non-metal (C, Si, B) allows HTES of carbides, silicides, and borides of tungsten [7, 9].

In the present work, studies results of the boron oxide effect on platinum-oxygen and tungsten electrodes in sodium tungstate melt and of the electrochemical behavior of this melt were presented. The electrochemical behavior of (and electrodeposition from) Na2WO4-B2O3 melts, the electrodeposition of tungsten coatings from them, as well as their physicochemical and operational properties, were determined. The study of electrochemical behavior of platinum-oxygen and tungsten electrodes in the Na_2WO_4-B_2O_3 melts made it possible to confirm the capability of the melts model with the formation of ditungstate ions and the possibility of realization of

multi-electron equilibria with these ions participation. The interest to this work was determined by the following: (a) a significant influence of boron oxide is observed onto the structure of cathodic deposits obtained from molybdenum containing melts [10-14]; (b) on the base of peculiarities of tungstate melts nature and structure, one can expect the better solubility and less fugacity of boron oxide than was observed in halide melts [10]; (c) boron oxide forms oxo-acid particles able to influence the acid-base interactions in tungstate melts [6].

RESULTS AND DISCUSSION

In the present work the effect of boron oxide on platinum-oxygen and tungsten electrodes in sodium tungstate melt.

The variation in activity of the melt components is not only of theoretical but also of practical interest in tungsten electrodeposition and synthesis of tungsten borides. Potentiometry was employed for the study under equilibrium conditions. The electromotive force (emf) of the following cells was measured:

$$Pt, O_2 \mid (1\text{-}x)\ Na_2WO_4 - xB_2O_3 \mid Na_2WO_4 - 0.2\ WO_3 \mid O_2, Pt \quad (1)$$

$$W \mid (1\text{-}x)\ Na_2WO_4 - xB_2O_3 \mid Na_2WO_4 - 0.2\ WO_3 \mid O_2, Pt \quad (2)$$

where x is the mole fraction of B_2O_3 in the melt.

1. Electrochemical behavior of platinum-oxygen and tungsten electrodes in the Na_2WO_4-B_2O_3 melt

The emf of cells (1) and (2) was measured at 1173 K varying the concentration of B_2O_3 in the range of 0-10 mol.% (the corresponding samples of B_2O_3 added to molten Na_2WO_4). The equilibrium potentials were established within 2-3 h judging by constancy of their final value to within 0.005 V for 1 h.

The variation of the oxygen electrode potential in Na_2WO_4-B_2O_3 melts (Fig. 1) can be explained in terms of the model we proposed for ion composition of such systems.

The expression for oxygen-electrode steady potential is written as follows:

$$1/2\ O_2 + 2e^- \leftrightarrow O^{2-} \quad (3)$$

$$E_{O^{2-}/O_2} = E^0_{O^{2-}/O_2} + \frac{2.3RT}{2F}\log\frac{P_{O_2}^{1/2}}{\left[O^{2-}\right]} \quad (4)$$

or, taking into account the constant partial pressure of oxygen over the melt, as:

$$E_{O^{2-}/O_2} = E^*_{O^{2-}/O_2} + \frac{2.3RT}{2F}\log\left[O^{2-}\right]^{-1} \quad (5)$$

The difference in potentials of the oxygen electrodes in cell (1) is described by the ratio of activities of oxygen ions in the melts, i.e.:

$$E = \frac{2.3RT}{2F}\log\left(a' / a''\right) \tag{6}$$

where: a'=activity of O^{2-} and a''=activity of O_2

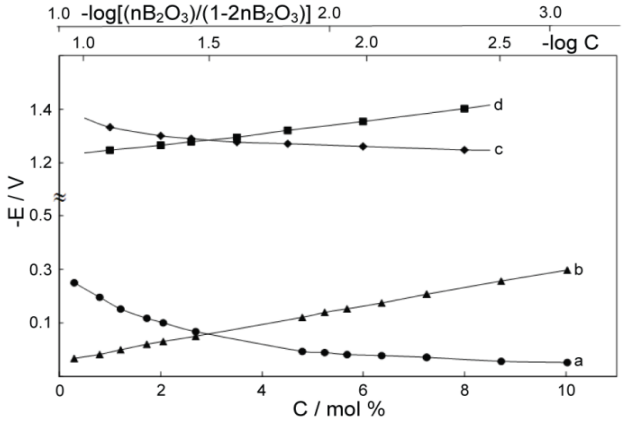

Figure 1. Dependence of potentials of platinum-oxygen (a) and tungsten (c); electrodes on B_2O_3 concentration and their analysis in the logarithmic coordinate system: (b) – platinum-oxygen electrode; (d) – tungsten electrode. (T = 1173 K).

In the neat tungstate melt there is the equilibrium:

$$(W_2O_7)^{2-} + O^{2-} = 2\,(WO_4)^{2-} \tag{7}$$

with the constant $K = \frac{[n(WO_4)^{2-}]^2}{[n(O)^{2-}][n(W_2O_7)^{2-}]}$ and n = the fraction of all species $[n(WO_4)^{2-}]$, $[n(W_2O_7)^{2-}]$, $[n(O)^{2-}]$ taking part in equilibrium (7). So the the tungsten ion balance can be written as follows:

$$n(WO4)^{2-} + 2n(W_2O_7)^{2-} = 1 \tag{8}$$

For stoichiometric sodium tungstate $[n(WO_4)^{2-}] \approx 1$, $[n(O)^{2-}] = [n(W_2O_7)^{2-}] << 1$, we have from eq.(7):

$$[n(O)^{2-}] = 1/K^{1/2} \tag{9}$$

In the presence of B_2O_3 acting as an acceptor of oxygen ions the following reactions can occur in the sodium tungstate melt:

$$2\,(WO_4)^{2-} + B_2O_3 \leftrightarrow (W_2O_7)^{2-} + 2\,(BO_2)^{-} \tag{10}$$

$$2\,(WO_4)^{2-} + 2\,B_2O_3 \leftrightarrow (W_2O_7)^{2-} + 2\,(B_4O_7)^{2-} \tag{11}$$

The mole fractions of tungstate and ditungstate ions, as determined from the ion balance, are:

$$n\ (WO_4)^{2-} = 1\text{-}2n\ (W_2O_7)^{2-} = 1\text{-}\ 2n\ B_2O_3 \quad (12)$$

$$n\ (W_2O_7)^{2-} = n\ B_2O_3 \quad (13)$$

for reaction (10) and

$$n\ (WO_4)^{2-} = 1\ -\ 2n\ (W_20_7)^{2-}\ = 1\ -\ 4n\ B_2O_3 \quad (14)$$

$$n\ (W_2O_7)^{2-} = 2n\ B_2O_3 \quad (15)$$

for reaction (11).

Inserting (12), (13), and (14), (15) in Eq. (7) we obtain equation for mole fractions of oxygen ions involved in reactions (10) and (11):

$$[\frac{1}{n(O)^{2-}}] = \frac{[K \cdot nB_2O_3]}{[1-2n \cdot B_2O_3]^2} \quad (16)$$

$$[\frac{1}{n(O)^{2-}}] = \frac{[2K \cdot nB_2O_3]}{[1-4n \cdot B_2O_3]^2} \quad (17)$$

After insertion of (16) and (17) in (5), the final equations relating the oxygen electrode potential and the concentration of B_2O_3 take the form:

$$E_{O^{2-}/O_2} = E^{*}_{O^{2-}/O_2} + \frac{2.3RT}{2F}\log\frac{\left(K \cdot nB_2O_3\right)}{\left(1-2nB_2O_3\right)^2} = E^{**}_{O^{2-}/O_2} + \frac{2.3RT}{2F}\log\frac{\left(nB_2O_3\right)}{\left(1-2nB_2O_3\right)^2} \quad (18)$$

$$E_{O^{2-}/O_2} = E^{*}_{O^{2-}/O_2} + \frac{2.3RT}{2F}\log\frac{\left(2K \cdot nB_2O_3\right)}{\left(1-4nB_2O_3\right)^2} = E^{**}_{O^{2-}/O_2} + \frac{2.3RT}{2F}\log\frac{\left(nB_2O_3\right)}{\left(1-4nB_2O_3\right)^2} \quad (19)$$

According to equations (18) and (19), the slopes of the curves $E_{O^{2-}/O_2} - \log[nB_2O_3/(1-2nB_2O_3)^2$ and $E_{O^{2-}/O_2} - \log[nB_2O_3/(1-4nB_2O_3)^2]$ at 1173 K should be 0.116 and 0.035 V, respectively. The experimentally determined slope for the first curve is 0.111-0.120 V (Fig. 1) whereas in the second semi-log coordinates the data points do not give a straight line. This suggests the occurrence of reaction (10) in the studied range of B_2O_3 concentration and the validity of the model used.

The constant K was estimated by solving eq. (18) with two values of the oxygen electrode potential, for stoichiometric sodium tungstate and the melt (Na_2WO_4-1 mol.% B_2O_3). The calculations give K = 108.6, $E^{*}_{O^{2-}/O_2} = -1.06$ V

and $nO^{2-} = 10^{-4.3}$. These values are in good agreement with the corresponding parameters found for Na_2WO_4 melts containing WO_3 and MoO_3 [3, 5].

The emf of cell (2) was measured, varying the concentration of B_2O_3 in the range of 0.5-10.0 mol.% with a small monocrystalline tungsten bar hung up by a platinum wire as an indicator electrode. The measurements were performed by the same procedure as for the oxygen electrode. At B_2O_3 concentration < 0.5 mol.% the chemically pure tungsten electrode undergoes corrosion because of which the measured emf values are nonreproducible. The corrosion is suppressed at $[B_2O_3] > 0.5$ mol.%.

The tungsten electrode potential is created by the reactions:

$$(WO_4)^{2-} + 6e^- = W + 4\ O^{2-} \quad (20)$$

$$4\ (W_2O_7)^{2-} + 6e^- = W + 7\ (WO_4)^{2-} \quad (21)$$

for tungsten in equilibrium with tungstate or ditungstate ions, respectively. The number of electrons per electroactive particle was estimated to be 1.5 from the slope of the $dE - d\log C_{B_2O_3}$ curve in the range of 0-5-10 mol.% B_2O_3 (Fig. 1). This value corresponds to reaction (21).

The possibility of reactions (10) and (11) is confirmed by the results of our thermodynamic calculations and of studies of the frozen $Na_2WO_4 – B_2O_3$ melts structure. The Gibbs free energy of reactions (10) and (11) at 1200 K is -112.67 kJ and -56.53 kJ, respectively. IR spectra of frozen melts confirm the ditungstate ions compounds presence.

2. Electroreduction of tungsten (VI) in Na_2WO_4-B_2O_3 melts

The reduction wave was observed at 1.1-1.3 V in stationary and nonstationary voltammograms of the tungstate melts containing B_2O_3 (Fig. 2). The limiting currents are proportional to the concentration of B_2O_3 rather than to the total concentration of tungsten in the melt. The major wave is preceed by an alloy-formation wave. To exclude the alloy formation we used a silver cathode which does not interact with tungsten. As the concentration of B_2O_3 is raised, the major wave becomes more intense and is displaced to positive potentials. At the same time it takes a sickle-shaped form. The reduction process proceeds in one step at any electrode polarization rate up to 10 V/s. The product of the potentiostatic electrolysis at the potential of –1.2 V is tungsten metal.

The plots of peak current versus B_2O_3 concentration at different polarization rates are linear (Fig. 3).

The values of $i_p/v^{1/2}$ are nearly constant over a wide range of polarization rates (0.05-2.0 V/s) (Fig. 4).

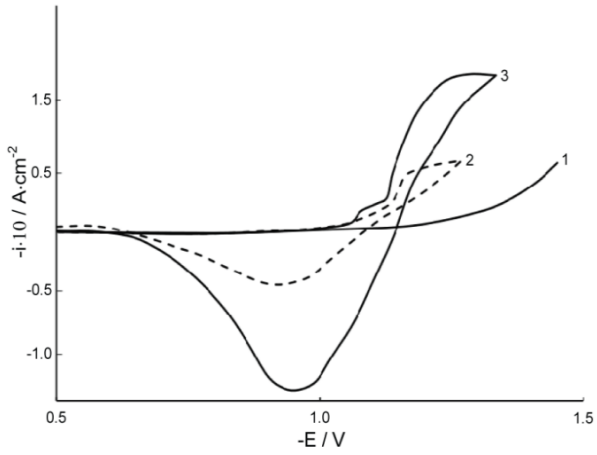

Figure 2. Voltammetric dependencies of Na_2WO_4 melt (1) when added sequentially B_2O_3: (2) – $1 \cdot 10^{-4}$ mol/cm^3; (3) – $8 \cdot 10^{-4}$ mol/cm^3;T = 1173 K, cathode – Pt, v = 0.1 V/s.

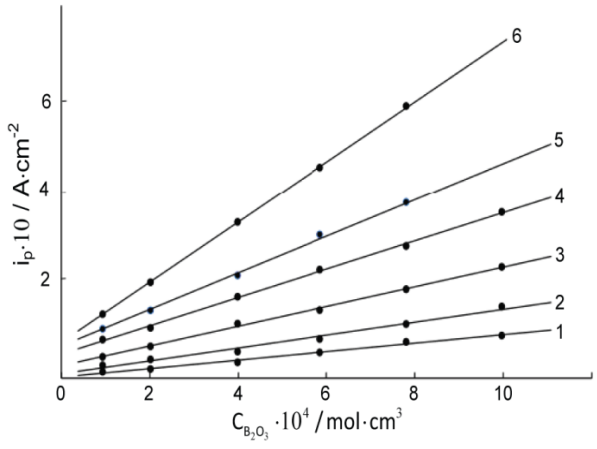

Figure 3. Dependence of the peak current on the B_2O_3 concentration at different polarization speeds: (1) – 0.02 V/s; (2) – 0.05 V/s; (3) – 0.1 V/s; (4) – 0.5 V/s; (5) – 1.0 V/s; (6) – 2.0 V/s ;T = 1173 K.

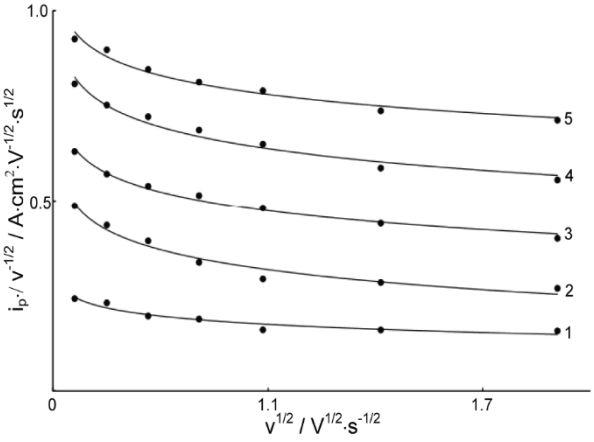

Figure 4. Dependence $i_p/v^{-1/2}$ – $v^{1/2}$ for the tungsten-containing ions electroreduction process at $C(B_2O_3)\cdot10^4$ mol/cm^3: (1) – 2 mol/cm^3; (2) – 6 mol/cm^3; (3) – 8 mol/cm^3; (4) – 10 mol/cm^3; (5) – 12 mol/cm^3; T = 1173 K.

The kinetic constant for stationary waves, $i_p/nFC = (0.7\text{-}1.0)\cdot10^{-4}$ cm/s, characterizing the transport of the reacting substances to the electrode surface is comparable to the values of χ for diffusion migration.

All these data suggest that the electrode process is limited by diffusion of electroactive species to the electrode, that is, under polarization conditions used, the rate of generation of the species is not the limiting factor.

The nature of the waves can be explained in terms of the acid-base interaction concept and the model we proposed earlier for the ionic composition of the melts in [6, 8]. The following equilibrium is established in the tungstate melt:

$$2\ (WO_4)^{2-} \leftrightarrow (W_2O_7)^{2-} + O^{2-} \tag{22}$$

with the equilibrium constant:

$$K = \frac{\left[WO_4^{2-}\right]^2}{\left[W_2O_7^{2-}\right]\left[O^{2-}\right]} \tag{23}$$

From the reported value of $K \approx 10^{10}\text{-}10^{12}$ [6, 8], the concentration of electroactive species $(W_2O_7)^{2-}$ was estimated to be in the range of $10^{-5}\text{-}10^{-4}$ mol % that is much lower than the voltammetry sensitivity limit. Because of this no waves were observed in the neat tungstate melt.

Boron oxide acting as an acceptor of oxygen ions displaces equilibrium (22) to the right increasing thereby the concentration of $(W_2O_7)^{2-}$ in the melt by eq.(10). The decrease in activity of oxygen ions in the presence of B_2O_3 added to the tungstate HTIL was studied on the platinum-oxygen electrode under equilibrium conditions. With boron oxide introduced in the HTIL, the concentration of $(W_2O_7)^{2-}$ increases and the system exhibits electrochemical activity at more positive potentials. The overall electrode process under these conditions can be presented by the equation (21). In order to elucidate the nature of the charge-transfer step (21) and to determine the number of electrons taking part in the electrode process, the stationary current-potential curves were presented in semilog coordinates log (i_d - i) - E (Fig. 5).

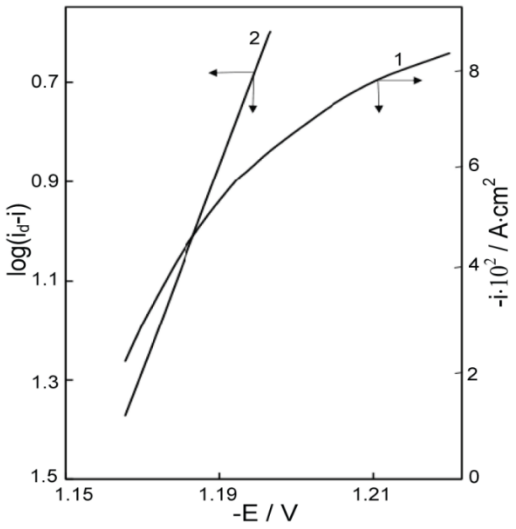

Figure 5. Cathodic polarization of tungsten electrode (1) and its analysis in the semi-logarithmic coordinate system (2);v = 0.02 V/s, T = 1173 K, $C(B_2O_3) = 6 \cdot 10^{-4}$ mol/cm^3.

In view of the sickle-shaped form of the stationary waves, the Kolthoff-Lingame equation was used. The slope of the log(i_d - i) - E curves at different B_2O_3 concentrations was found to be 37-44 mV and n = 5.3-6.2. The theoretical slope for a six-electron reversible reaction is 39 mV. A good agreement between the experimental and theoretical values testifies that the charge-transfer step (21) is reversible. This inference is confirmed by the following experimental facts: the deposition potential and the half-wave potential are independent of the polarization rate up to 0.2 V/s; the concentration dependence of the potential for equilibrium (21) is well described by the Nernst equation.

We determined the number of electrons involved in the electrode process also from the equation for nonstationary current-potential curves:

$$E_{p/2} - E_p = 2.2RT/nF \quad (24)$$

The result at different B_2O_3 concentrations and polarization rates (0.05-0.2 V/s) is n = 5.6-6.1.

At higher polarization rates (v > 0.5 V/s) the reversible process becomes quasi-reversible as shown by deviation of the $i_p /v^{1/2}$ relationship from linearity *vs.* $v^{1/2}$ and the dependence of E_p and $E_{p/2}$ on the polarization rate.

3. Electrodeposition of tungsten coatings, their physicochemical and operational properties.

3.1. Electrodeposition of tungsten coatings by electrolysis of tungsten-borate melts

For successful coating, it is important that the corrosion potential is higher than the deposition potential. Therefore, to assess the possibility of coating nickel, various steels, and titanium (usually, tungsten is not deposited on these metals from halide and halide-oxide melts), the stationary potentials of these metals relative to the $Na_2WO_4 – 0.2WO_3 \mid O_2$, Pt half-element (table 1) were measured. The deposition potential of tungsten is lower than the corrosion potentials of nickel, ST3, stainless steel, which opens up the possibility of good coatings. The stationary potential of titanium was not established for a long time and changed abruptly. Apparently, this is due to the formation of low-valence titanium oxides. Therefore, before the deposition of tungsten, titanium was nickel-plated or nitrided.

Table 1. Free corrosion potentials (E_{cor}) of nickel, ST3, stainless steel 12X18H10T and deposition potential (E_{dep}) of tungsten in tungstate-borate melts Na_2WO_4 – 5 mol% B_2O_3.

E_{cor}, V			E_{dep}, V
Ni	**ST3**	**Steel 12X18H10T**	
-1.17	-1.31	-1.30	-1.5
-1.22	-1.35	-1.3	-1.75

We have studied the effect of boron oxide concentration, temperature, cathode current density, and electrolysis duration on the composition and structure of cathodic deposits, optimal parameters of reverse deposition of tungsten from Na_2WO_4 - B_2O_3 melts were selected.

Tungsten precipitates if the concentration of boron oxide does not exceed 10 mol %, at a higher concentration, tungsten and bronze oxides are found on the diffractograms. Tungsten precipitates if the concentration of boron oxide does not exceed 10 mol %, at a higher concentration, tungsten bronze (M_xWO_3), where M denote monovalent cation and x is in the range 0 to 1 [15]. Solid coatings were obtained at 1073-1323 K and current densities up to 10 A/dm^2.

The higher the electrolysis temperature, the coarser the precipitate is. However, at a temperature of 1073 K, tungsten layers no thicker than 10 μm are obtained, which are not sufficiently adhered to the substrate. At temperatures below 1073 K and current density above 50 A/dm^2, a highly dispersed powder with a specific surface area up to 30 m^2/g will precipitate.

The effect of cathode density, electrolysis duration, and reverse mode parameters was studied in (Na_2WO_4 + 5 mol % B_2O_3). Well-adhered, uniform, continuous, absolutely pore-free coatings were obtained at a temperature of 1173 K and a current density of 1-10 A/dm^2. In the initial period of deposition, the size of deposit crystallites decreased with increasing current density. However, at a density above 10 A/dm^2, the grain became significantly coarser, the roughness amplitude increased from 1 to 2–3 μm, and the progressive growth of individual protrusions turned into dendrite formation, which prevented further thickening of the coating. Below 1 A/dm^2, the corrosion rate of the substrate exceeds the rate of tungsten deposition, causing poor adhesion of the coatings. The rate of tungsten deposition in the studied range of current densities is 15–40 μm/h, the current efficiency of tungsten is 85% (Fig. 6). As the duration of electrolysis increases, the current efficiency decreases (Fig. 7).

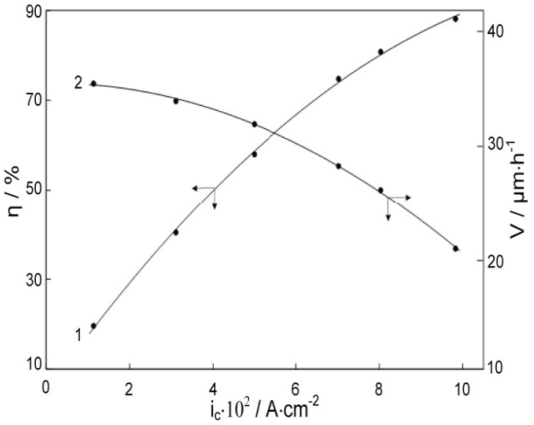

Figure 6. Dependence of the tungsten coating deposition rate (1) and the yield of tungsten by current (2) on steel samples from the cathodic current density; T = 1173 K.

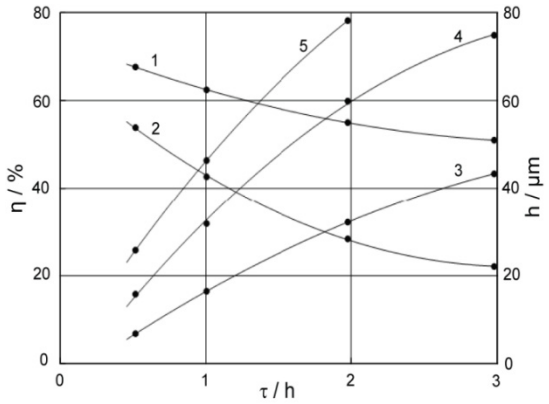

Figure 7. The dependence of the thickness of the tungsten coating (1-3) and the yield of tungsten according to the current (4) and (5) on steel samples from the duration of electrolysis at the current density: (1) and (4) – 4 A/dm^2; (2) and (5) – 6 A/dm^2; (3) – 8 A/dm^2;T = 1173 K.

With thickening of the coating, the structure of its surface changes from finely crystalline with a uniform grain to coarse-grained. The SEM images of the tungsten deposit on steel depending on electrodeposition time and the current density in Fig.8. As one can see the deposit change from homogenous low small grains to enough homogenous large-grained with deposition time and current density. To obtain a fine-grained structure, a reverse electrolysis mode was used. The ratio t_k:t_a was changed within 20 - 40, the duration of the anodic phase is 0.5-2.0 s, the anodic current density is 15 - 50 A/dm^2. To obtain a coating, the following electrolysis parameters are optimal: t_k = 20 s, t_a = 0.5-1.0 s, i_k = 8-10 A/dm^2, i_a = 15-30 A/dm^2. This way of doing electrolysis leads to reducing the roughness of the coatings by half, as well as increasing their thickness to 200 µm.

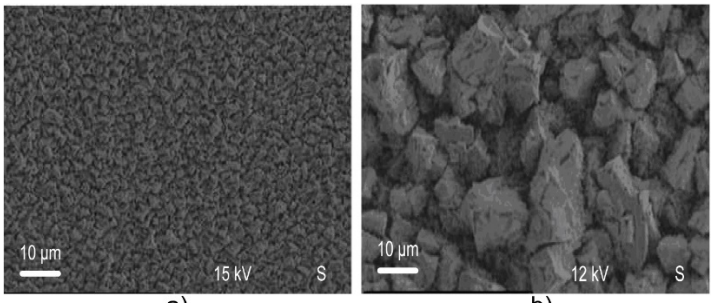

Figure 8. SEM image of tungsten coating deposited on steel substrate: a) 20 s; 8 A/dm^2; b) 60 s, 15 A/dm^2.

3.2. Physico-chemical and operational properties of tungsten coatings

Solid tungsten coatings on graphite, nickel, copper, molybdenum, tungsten, machine-building structural steels, heat-resistant and tool hard alloys, on nitrided and nickel-plated titanium have been obtained.

Under laboratory conditions, alundum containers, tungsten plates or rods were used as anodes, and chemically pure initial components. In the resulting tungsten coatings, X-ray microanalysis revealed impurities (Al, Cr, Mo, Ni) within only $2 \cdot 10^{-2}$ - $4 \cdot 10^{-4}$ wt. %. Such a content of impurities does not noticeably affect the structure of the coatings. An indirect criterion for the high adhesion strength of a coating to a substrate is the absence of its peeling during qualitative tests.

The porosity of the coating was determined by applying filter paper impregnated with a 10 g/l solution of $K_3Fe(CN)_6$ + 20 g/l NaCl on coated steel ST3 and 45. Test duration was 5 min. The average number of pores per 100 cm^2 of the surface was 5-6. According to the evaluation standards (ASTM B809), the pore area is 0.0–0.1%, which corresponds to practically pore-free coatings [16]. The microhardness of the coating is 4.3-4.5 GPa. The layers of the base adjacent to the coating are noticeably strengthened, which indicates the mutual diffusion of the elements of the coating and the base. A diffusion zone with a length of 10-15 μm is shown by X-ray microanalysis of a transverse section of ST3 coated with tungsten.

Wear resistance tests were carried out on an SMC-2 instrument at a specific load of 5 MPa in transformer oil in a wide range of sliding speeds. The counterbody is hardened steel 45. The coating increased wear resistance by 4-6 times.

For abrasive resistance, steel 45 samples with coatings were tested in the medium of a fraction of 150 μm of electrocorundum at a load of 44.1 + 0.25 N. Due to the coating, the wear resistance increased by a factor of 3-5 and was only slightly inferior to the resistance of samples borated from the gas phase.

Thus, we have studied the electrochemical behavior of tungstate-borate melts, mastered the electrodeposition of tungsten coatings and their properties.

CONCLUSIONS

The study of electrochemical behavior of platinum-oxygen and tungsten electrodes in the Na_2WO_4-B_2O_3 melts made it possible to confirm the capability of the HTILs model with the formation of ditungstate ions and the possibility of realization of multi-electron equilibrium with these ions participation.

According to the electrochemical measurements results, namely, due to the linear dependence of the peak current of ditungstate ion reduction waves

on the concentration of B_2O_3, to the constancy of the values of the ratio of the peak current to the square root of the polarization speed, as well as to the values of the kinetic constants, electrode process is limited by diffusion of electroactive species to the electrode. Under polarization conditions used, the particles species generation rate is not the limiting factor.

A good agreement between the experimental and theoretical numbers of electrons taking part in the electrode process testifies that the charge-transfer step of ditungstate-ion electroreduction is reversible. This inference is confirmed by the experimental facts that the deposition potential and the half-wave potential are independent of the polarization rate up to 0.2 V/s, and that the concentration dependence of the equilibrium potential of tungsten electrode within melt is well described by the Nernst equation.

The influence of boron oxide concentration, temperature, cathodic current density, and duration of electrolysis on the composition and structure of cathodic deposits was studied. The coatings were obtained in the temperature range of 1073-1323 K at a current densities up to 1-10 A/dm^2, if the concentration of B_2O_3 does not exceed 10 mol %. A reversible deposition mode was used to obtain a fine crystal structure.

Electrolysis of Na_2WO_4-B_2O_3 melts produced continuous nonporous tungsten coatings on graphite and metal materials. The speed of their deposition was up to 15-40 μm/h, the current yield was up to 85%, the thickness was up to 100 μm in the direct current mode of deposition and up to 200 μm in the reverse mode of deposition.

The microhardness of the coatings is 4.3-4.5 GPa. As a result of their deposition the wear resistance of steel materials increases by 4-6 times, and abrasive resistance by 3-5 times.

EXPERIMENTAL

The platinum-oxygen reference electrode was semi-dipped in the melt of constant composition, Na_2WO_4 - 20 mol % WO_3, separated from the main electrolyte with an alundum jacket 6-8 mm in diameter playing the role of a diaphragm. The open end of the jacket communicated with the atmosphere. Potentiometric measurements were carried out in air ($P_{O_2} = 21.3$ kPa). Such electrodes are widely used in oxide melts, specifically in tungstate systems [17, 18].

Investigations of Na_2WO_4-B_2O_3 melt electrochemical behavior were carried out in the three-electrode quartz electrochemical cell at 1173 K. Used methods of investigation – single and multi cycle voltammetry. Voltammetric curves were registered with the pulse potentiostat PI-50-1

As anode and at the same time as the melt container the platinum crucible was used. As indicator electrodes were used semi-dipped and full dipped needle platinum and silver and tungsten electrodes (wire diameter 0.5-1.0 mm, square of electrodes was 0.1-0.3 cm^2). As reference electrode a platinum-oxygen electrode 0.8 Na_2WO_4-0.2 WO_3/O_2,Pt was used [17]. Diagnostics and estimation of electrode processes kinetic parameters was carried out according to the theory of stationary and non-stationary electrode processes [19]. Systems for the tungsten coatings electrochemical deposition were based on Na_2WO_4-B_2O_3 melt. As anode a tungsten plates in alundum container or graphite crucibles was used and as cathodes – plates of metals for electrodeposition (10×20×1 mm).

The thickness and deposition rate of coatings at the surface of plane-parallel plates were assessed by gravimetric and metallographic methods, as well as using a VTO-25 micrometer and 2IGM detector [20,21].

REFERENCES

1. J. S. Wilkes; *Green Chem*., **2002**, *4*, 73-80.
2. A. Nishikata; H. Numata; T. Tsuru; *Mater. Sci. Eng*: *A*, **1991**, *146*, 15-31.
3. V. V. Malyshev; H. B. Kushkov; V. I. Shapoval; *J. Appl. Electrochem*., **2002**, *32*, 573-579.
4. V. L. Cherginets; *Russ. Chem. Rev*., **1997**, *66,* 597-611.
5. V. L. Cherginets; *Oxoacidity: Reactions of Oxo-compounds in Ionic Solvents*, N. J. B Green; Ed.; Netherland: Elsevier Science, **2005**. ISBN: 978-0-444-51782-1
6. V. A. Onischenko; V. V. Soloviev; L. A. Chernenko; V. V. Malyshev; S. N. Bondus; *Materialwiss. Werkst*., **2014**, *45*(11), 1030-1038.
7. V. V. Malyshev; V. V. Soloviev; L. A. Chernenko; V. N. Rozhko; *Materialwiss. Werkst*., **2015**, *46*(1), 5-9.
8. V. Malyshev; A. Gab; A. M. Popescu; V. Constantin; *Chem. Res. Chin. Univ*. **2013**, *29*, 771-775.
9. V. Malyshev; D. Shakhnin;A. Gab; I. Astrelin; L. Molotovska; V. Soare; C. Donath; E.I. Neacsu; V. Constantin; A.M. Popescu; *Rev. Chim. (Bucharest)*, **2016**, *67*(12), 2490-2500.
10. V. Danek; *Physico-chemical analysis of molten electrolytes*, Amsterdam: Elsevier Science, **2006**.
11. S. K. Ghosh; J. Varshney; A. Srivastava; Ch. Srivastava; *J. Electrochem. Soc*., **2021**, *168*(4), 046502.
12. W. Jin; Ch. Ge; Q. Kou; P. Jiang; S. Xiao; *Int. J. Electrochem. Sci*., **2021**, *16*(3), 210311.
13. V. Malyshev; A. Gab; D. Shakhnin; C. Donath; E. I. Neacsu; A. M. Popescu; V. Constantin; *Rev. Chim. (Bucharest)*, **2018**, *69*(9), 2411-2415.

14. V. Malyshev; A. Gab; D. Bruskova; T. Dmytrenko; M. Gaune-Escard; *Nano Studies*., **2019**, *19*, 77-86.
15. J. D. Guo; M. S. Whittingham; *IJMP B,* **1993**, *7,* 4145-4164.
16. ASTM B809, Standard test method for porosity in metallic coatings by humid sulfur vapor ("Flowers-of-Sulfur"), ASTM International, West Conshohocken, PA, **2016**, (2018).
17. G. Inzelt; A. Lewenstam; F. Scholz; *Handbook of Reference Electrodes*, Berlin, Heidelberg: Springer-Verlag, **2015**. ISBN: 978-3-642-44873-7.
18. A.I. Bhatt; G.A. Snook; *Reference electrodes for ionic liquids and molten salts*, in: G. Inzelt; A. Lewenstam; F. Scholz; (Eds). *Handbook of Reference Electrodes*. Berlin, Heidelberg: Springer-Verlag, **2013**, 189-227. ISBN: 978-3-642-36187-6.
19. C. G. Zoski; Ed., *Handbook of electrochemistry*, Amsterdam: Elsevier Science, **2006**. ISBN 978-0-444-51958-0.
20. V. Malyshev; D. Shakhnin; A. Gab; M. Gaune-Escard; I.M. Astrelin; Effect of electrolysis parameters on the coating composition and properties during electrodeposition of tungsten carbides and zirconium diborides, cap. 4.8, pag.295, in Molten Salts Chemistry and Technology, First ed., Marcelle Gaune-Escard; Geir Martin Haarberg; (Eds.). **2014,** John Wiley & Sons, Ltd.
21. V. Malyshev; N. Kushchevska; G. Bagliuk; D.Shakhnin; O. Paprotskaya; V. Kurovskyi; *Int. Sci. J. Mach. Tech. Mater*., **2018**, *12*(7), 302-304.